Semiconductor Physics, Quantum Electronics & Optoelectronics, 2008. V. 11, N 2. P. 178-187.

PACS 81.16.Nd, 85.40.Hp

Finding of the optimal parameters of animated and stereographic rainbow diffractive images

I.S. Borisov[1], V.I. Girnyk[2], S.A. Kostyukevych[3], V.I. Grygoruk[1], K.V. Kostyukevych[3]
1 - Taras Shevchenko Kyiv National University, Ukraine
2 - Optronics PC, Kyiv, Ukraine
3 - V. Lashkaryov Institute of Semiconductor Physics NAS Ukraine, Kyiv, Ukraine
41, prospect Nauky, 03028 Kyiv, Ukraine, Phone: (380-44) 525-62-05; e-mail: sekret@spie.org.ua

Abstract. We have considered the basic aspects of the technology of animated and stereographic rainbow images. These images can be included in Optical Security Devices (OSDs) in order to increase their structure complexity and to improve their protective properties. The cited technology provides, on the one hand, a simple identification on the visual level of verification and, on the other hand, the sufficient reliability against counterfeits. The last property is achieved at first by the division of the elemental unit on elemental regions of any adjusted shape with outline of the precision that is inaccessible for the recreation without Electron Beam Lithography Equipment (EBLE) which is used for the recording of OSDs. Second, the used encoding methods also assure the certain reliability.

In the context of the paper, the theoretical discussion based a quantitative formulation of the Huygens--Fresnel law of the diffraction on an elemental diffractive grating is carried out. For other definite Conditions of Lighting and Observation of Diffracting Light (CLODL), the correlation between the slope angle of diffraction grating strokes and the corresponding horizontal parallax angle is got; and the parameter which defines the channel selection (the quality of splitting into separate channels) is introduced. The rule for the definition of the wavelength and the intensity of light that diffracts on a given grating under certain CLODL is derived as well. This fact allows one to create the software utility that models the behavior of anigrams or stereograms.
An algorithm of the synthesis of anigrams and stereograms as parts of OSDs using the technology of a composite "figure" elemental unit (that is composed from parts of any shape) and applying the halftone encoding by the period, filling, and achromaticity or all these parameters at once is elaborated, and its software implementation is constructed. The criteria for the choice of such anigram's parameters as the resolution, number of channels, and angle distances between them are elaborated. In order to check them, the results of tests are summarized. The investigation of the optimal parameters of halftone images' encoding finding is implemented, and the results obtained for the tough and flexible linkings of a channel to the subregion of an elemental unit for hatching images are compared.

Keywords: optical security devices, electron beam lithography, anigram, stereogram.

Manuscript received 31.03.08; accepted for publication 15.05.08; published online 30.06.08.

1. Introduction

The application of OSDs as a reliable inexpensive means of protection of values, documents, and goods against counterfeits acquires a great spreading for the last time. So the problem of raising the OSD's protective properties becomes more and more topical. One of the ways of solving this problem is to increase the OSD's structure complexity. In order to attain this purpose, the methods of computer synthesis of stereographic or animated rainbow diffractive images were elaborated. Stereograms and anigrams are enough spectacular and

visually impressive. Stereograms are similar to the Computer-Generated Rainbow Holograms (CGRHs) of 3D images [1-9] both by the appearance and by the function and can be included as a component into OSDs of the polygram type [1]. The presented animated or stereographic images are entirely computer-generated and are recorded with the use of the EBLE [10-11]. The technique of stereograms is based on the principle of the human vision physiology of 3D visual perception – the principle of binocular stereoscopy. The sequence of angle shots of a 3D scene is encoded into the diffractive structure of a holographic stereogram with the space-division method. The theory and the means of this encoding are presented in the following sections.

2. Theoretical basis of the construction of multiplex diffractive images

2.1. Theory of the diffraction on an elemental diffractive grating.

In this section, we discuss how the reflective phase Elemental Diffractive Grating (EDG) works. Let us introduce a left-sided right-angled Cartesian coordinate system (CCS), whose center coincides with the center of the considered planar EDG, and the Ox axis is perpendicular to the SOP plane, where SO is the incidence beam and OP is the diffracting beam. Thus, the SO and OP beams lie in the yOz plane. Let the angle which lies aside clockwise from the Oz axis to the incidence beam OS under observation from the semispace of the positive x be denoted as φ_0, and let the angle which lies aside counterclockwise from the Oz axis to the diffracting beam OP under observation be denoted as φ (Fig. 1).

Let the Oz' axis be constructed parallel to the normal to the front side of the EDG plane (see Fig. 2). Then we denote the line of intersection of the EDG plane with the zOx plane as Ox' and select the Ox' axis

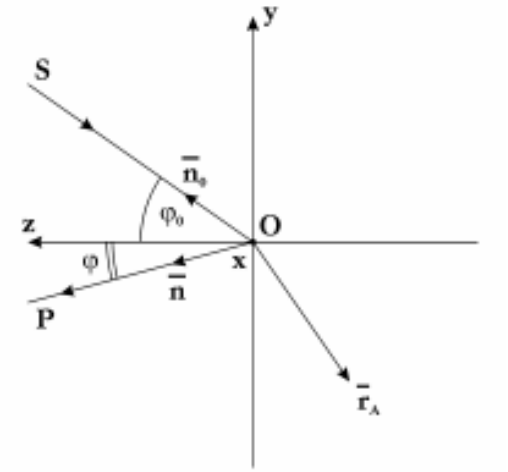

Fig. 1. Incidence-diffraction plane

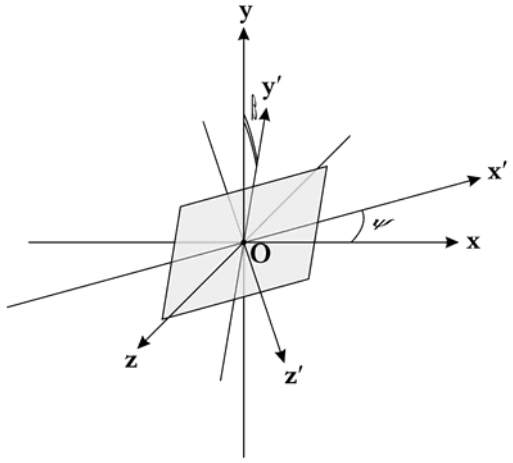

Fig. 2. Space disposition of EDG.

direction in such a way that the axes Oz', Oy, and Ox' compose the left-sided CCS. Let the angle which lies aside counterclockwise from the Ox axis to the Ox' axis under observation from the semispace of the positive y be denoted as ψ. Let the projection of the Oy axis on the EDG plane be denoted as Oy'; let the Oy' axis direction be selected in such a way that the axes Oz', Ox', and Oy' compose the left-sided CCS. As β, we denote the angle which lies aside counterclockwise from the Oy axis to the Oy' axis under observation from the semispace of the positive x'.

And, finally, let the angle which forms the line of an EDG's stroke with the Ox' axis be designated as γ. Next, let the $Ox''y''z''$ CCS be formed by rotating the $Ox'y'z'$ CCS by the angle γ counterclockwise under observation from the semispace of the positive z'.

Figure 3 shows the topology of the EDG structure in its relative plane ($Ox'y'$ or $Ox''y''$) and the EDG's stroke profile that is set by the function $F_n(y'', z'') = 0$ on the interval $n \cdot d \le y'' < (n+1) \cdot d$, where d is the EDG period.

Fig. 3 shows the topology of EDG structure in its relative plane ($Ox'y'$ or $Ox''y''$) and EDG's stroke profile that is setting by the function $F_n(y'', z'') = 0$ on the interval $n \cdot d \le y'' < (n+1) \cdot d$, where d is the EDG period.

After the geometry of a space disposition of the EDG relative to the incident and diffractive beams is determined, as well as geometric parameters of the EDG itself are defined, we proceed to the finding, first, the optical path difference $\Delta(x'', y'', z'')$ between the incident and diffractive beams as components of the given incident and diffracting waves at the point $A(x'', y'', z'')$ and at the point $O(0,0,0)$ of the diffractive structure, and, second, the area df_n perpendicular to the incident

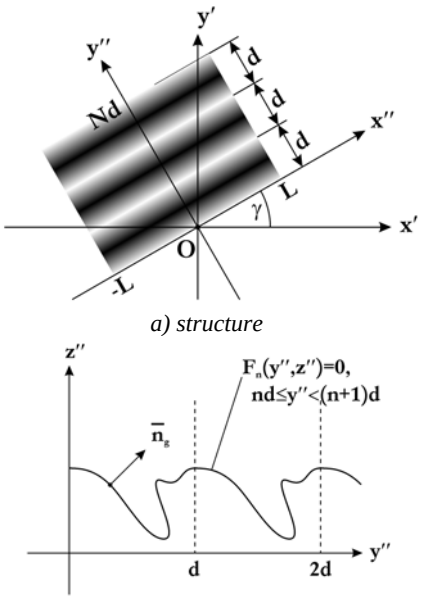

a) structure

b) profile

Fig. 3. EDG's topology

beam which is cut by the bundle of rays that diffract on the EDG's surface elemental fragment, which is projected on the $x''Oy''$ plane as the $\{\ x_0'' \le x'' < x_0'' + dx'',\quad y_0'' \le y'' < y_0'' + dy''$ rectangle.

The optical path difference $\Delta(x, y, z)$ can be found (see Fig. 1) as::

$$\Delta(x, y, z) = -\vec{n}_0 \cdot \vec{r}_A - \vec{n} \cdot \vec{r}_A\,, \tag{1.1}$$

where

$$\vec{n}_0 = \{0, \sin\varphi_0, \cos\varphi_0\ \},\ \vec{n} = \{0, -\sin\varphi, \cos\varphi\ \},$$
$$\vec{r}_A = \{x, y, z\}; \tag{1.2}$$

i.e.:

$$\Delta(x, y, z) = -y(\sin\varphi_0 - \sin\varphi) - z(\cos\varphi + \cos\varphi_0)\,. \tag{1.3}$$

Let us consider the conversions of coordinates:

$$\begin{cases} x = x'\cos\psi + y'\sin\beta\sin\psi + z'\cos\beta\sin\psi\,, \\ y = y'\cos\beta - z'\sin\beta\,, \\ z = -x'\sin\psi + y'\sin\beta\cos\psi + z'\cos\beta\cos\psi\,; \end{cases} \tag{2.1}$$

$$\begin{cases} x' = x''\cos\gamma - y''\sin\gamma\,, \\ y' = x''\sin\gamma + y''\cos\gamma\,, \\ z' = z''\,; \end{cases} \tag{2.2}$$

then we substitute (2.2) into (2.1) and get:

$$\begin{cases} x = x''(\cos\gamma\cos\psi + \sin\gamma\sin\beta\sin\psi\,) + \\ + y''(-\sin\gamma\cos\psi + \cos\gamma\sin\beta\sin\psi\,) + z'\cos\beta\sin\psi\,, \\ y = x''\sin\gamma\cos\beta + y''\cos\gamma\cos\beta - z''\sin\beta\,, \\ z = x''(-\cos\gamma\sin\psi + \sin\gamma\sin\beta\cos\psi\,) + \\ + y''(\sin\gamma\sin\psi + \cos\gamma\sin\beta\cos\psi\,) + z''\cos\beta\cos\psi\,. \end{cases} \tag{2.3}$$

Now, after putting (2.3) into (1.3), the expression $\Delta(x'', y'', z'')$ we are looking for can be found as:

$$k\Delta(x'', y'', z'') = \eta\, x'' + \nu\, y'' + \mu\, z'' \tag{3.1}$$

where $k = 2\pi/\lambda$ is the wave number, and the following designations are introduced:

$$\begin{cases} \eta = k\{-\sin\gamma\cos\beta\,(\sin\varphi_0 - \sin\varphi) + \\ + (\cos\gamma\sin\psi - \sin\gamma\sin\beta\cos\psi\,)(\cos\varphi + \cos\varphi_0)\}, \\ \nu = k\{-\cos\gamma\cos\beta\,(\sin\varphi_0 - \sin\varphi) - \\ - (\sin\gamma\sin\psi + \cos\gamma\sin\beta\cos\psi\,)(\cos\varphi + \cos\varphi_0)\}, \\ \mu = k\{\sin\beta\,(\sin\varphi_0 - \sin\varphi) - \cos\beta\cos\psi\,(\cos\varphi + \cos\varphi_0)\}. \end{cases} \tag{3.2}$$

Next, the df_n can be found (see Fig. 1 and Fig. 3,b) as:

$$df_n = \vec{n}_0 \cdot \vec{n}_g\, dx''dl'' \tag{4.1}$$

where

$$\vec{n}_0 = \vec{i}_2\sin\varphi_0 + \vec{i}_3\cos\varphi_0 \text{ and } \vec{n}_g = \vec{i}_2''\, c\frac{\partial F_n}{\partial y''} + \vec{i}_3''\, c\frac{\partial F_n}{\partial z''} \tag{4.2}$$

are, respectively, the normals to the back side of the front of the incident wave and to the front side of the elemental area of the EDG's surface (the $Oxyz$ and $Ox''y''z''$ CCS basis vectors are denoted as $\{\vec{i}_1, \vec{i}_2, \vec{i}_3\}$ and $\{\vec{i}_1'', \vec{i}_2'', \vec{i}_3''\}$, respectively),,

$$c = \left|\left(\frac{\partial F_n}{\partial y''}\right)^2 + \left(\frac{\partial F_n}{\partial z''}\right)^2\right|^{-\frac{1}{2}},$$

$$dl'' = \sqrt{dx''^2 + dy''^2} = \sqrt{\left(\frac{\partial F_n}{\partial y''}\right)^2 + \left(\frac{\partial F_n}{\partial z''}\right)^2}\left|\frac{\partial F_n}{\partial z''}\right|^{-1} dy''\,. \tag{4.3}$$

According to (2.3), we have:

$$\begin{cases} \vec{i}_2 \cdot \vec{i}_2'' = \cos\gamma\cos\beta, \\ \vec{i}_2 \cdot \vec{i}_3'' = -\sin\beta, \\ \vec{i}_3 \cdot \vec{i}_2'' = \sin\gamma\sin\psi + \cos\gamma\sin\beta\cos\psi\,, \\ \vec{i}_3 \cdot \vec{i}_3'' = \cos\beta\cos\psi\,, \end{cases} \tag{4.4}$$

so we get the relation:

$$df_n = \left|\frac{\partial F_n}{\partial z''}\right|^{-1}\Big[\cos\gamma\cos\beta\sin\varphi_0 +$$
$$+ (\sin\gamma\sin\psi + \cos\gamma\sin\beta\cos\psi\,)\cos\varphi_0\Big]\frac{\partial F_n}{\partial y''}dx''dy'' +$$
$$+ \left|\frac{\partial F_n}{\partial z''}\right|^{-1}\Big[-\sin\beta\sin\varphi_0 + \cos\beta\cos\psi\cos\varphi_0\Big]\frac{\partial F_n}{\partial z''}dx''dy'', \tag{4.5}$$

by putting consecutively (4.2), (4.3), and (4.4) into (4.1), or

$$df_n = g(y'', z'')dx''dy'', \tag{4.6}$$

where

$$\begin{cases} g(y'', z'') = \left|\dfrac{\partial F_n}{\partial z''}\right|^{-1}\left(c_1\dfrac{\partial F_n}{\partial y''} + c_2\dfrac{\partial F_n}{\partial z''}\right), \\ c_1 = \cos\gamma\cos\beta\sin\varphi_0 + \\ +(\sin\gamma\sin\psi + \cos\gamma\sin\beta\cos\psi)\cos\varphi_0, \\ c_2 = -\sin\beta\sin\varphi_0 + \cos\beta\cos\psi\cos\varphi_0. \end{cases} \tag{4.7}$$

According to the Huygens--Fresnel law in its quantitative formulation, any of the components of the electrical or magnetic field strength vectors $\vec{E}$ and $\vec{H}$ at the point P is defined by the following expression:

$$u_p = \int_\sigma \frac{k\,u_S}{2\pi i\,R^*}\exp\{ikR^*\}\rho\, df_n \ , \tag{5.1}$$

where $k = 2\pi/\lambda$ – wave number, u_S is the corresponding component of $\vec{E}$ or $\vec{H}$ vectors at the point S that is harmonically changing with the time t with the amplitude a and the angular frequency ω which can be written down in the complex-valued form as:

$$u_S = a\cdot\exp\{-i\omega t\}, \tag{5.2}$$

where i is the imaginary unity, df_n is the perpendicular to at elemental area of the incident beam which is cut by the falling bundle of rays that diffract on the EDG's surface elemental fragment, ρ is the reflectance of this area, R^* is the distance from the area df_n to the point P, σ is the surface of the EDG's fragment, the result of the diffraction on which is calculated.

Let us assume that the source S and the observer P are sufficiently far from the point O as compared with the EDG's sizes to consider both the incident and diffracting waves as plane waves. Then we can write down:

$$R^* = R + \Delta \approx R, \tag{5.3}$$

where R is the length of the segment OP, and Δ is the optical path difference between the beams that falls down and diffracts, respectively, as components of the given incident and diffracting waves on the area df_n and at the point O. By taking (5.3) into account, expression (5.1) acquires the following form:

$$u_p = \frac{k\,u_S\exp\{ikR\}}{2\pi i\,R}\int_\sigma \exp\{ik\,\Delta\}\rho\, df_n\,. \tag{5.4}$$

Let us put (3.1) and (4.6) into (5.4) and select the n-th EDG's stroke [the region that is set by the expressions $\{-L \le x'' < L,\ n\cdot d \le y'' < (n+1)\cdot d$ (see Fig. 3,a)] as a fragment, the result of the diffraction on which is calculated:

$$\begin{aligned} u_p &= A_1\int_{-L}^{L}\exp\{i\eta x''\}dx''\times \\ &\times \int_{nd}^{(n+1)d}\exp\{i\nu y'' + i\mu z''\}\rho(y'', z')\,g(y'', z'')dy'', \end{aligned} \tag{5.5}$$

where

$$A_1 = \frac{k\,u_S\exp\{ikR\}}{2\pi i\,R}. \tag{5.6}$$

The first integral in expression (5.5) can be calculated easily, but the second one cannot be found analytically except for the case of certain simplified shapes of the stroke profile $F_n(y'', z'') = 0$ and only for a certain simple function of the reflectance distribution $\rho(y'', z'')$. We will return to this issue in what follow and now just rewrite expression (5.5) without any loss of generality as:

$$\begin{aligned} u_p &= 2LA_1\frac{\sin\eta L}{\eta L}\times \\ &\times \int_{nd}^{(n+1)d}\exp\{i\nu y'' + i\mu z''\}\rho(y'', z')\,g(y'', z'')dy''. \end{aligned} \tag{5.7}$$

This relation describes the result of the diffraction on the one stroke of EDG. We are able now to draw certain conclusions already on this stage of the analysis of the diffraction on EDG. Indeed, since the remaining integral is a function of the stroke number n, so it is responsible for the transverse (across the stroke line – parallel to the Oy'' axis) inphasity of the diffraction on the stroke elements and for the reciprocal interaction of the strokes, i.e. for the selection of the diffracted light by wavelength. And vice versa, the $\frac{\sin\eta L}{\eta L}$ multiplier don't depend on n, and therefore it is the same for any stroke of EDG; hence it determines the longitudinal (along the stroke line – parallel to the Ox'' axis) inphasity of the diffraction on the stroke elements. In other words, it defines the selection of the diffracted light by the Horizontal Parallax (HP) angle ψ under the other constant Conditions of Lighting (of EDG by the white light) and Observation of the Diffracting Light (CLODL). The graph of the dependence of the diffracted light amplitude on the HP angle ψ or the indicatrix of the diffraction by the HP angle ψ the in normalized coordinates (ηL as an analog of ψ) – the function $\frac{\sin\eta L}{\eta L}(\eta L)$ – is depicted in Fig. 4. This function, i.e. the electromagnetic field amplitude, attains the maximum under condition $\eta = 0$, i.e. [see expression (3.2)] under the condition:

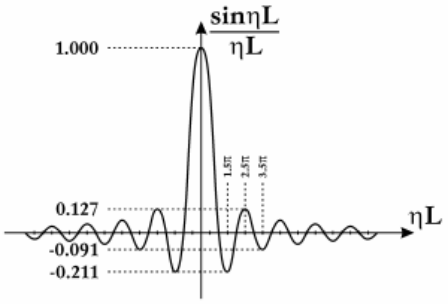

Fig. 4. Indicatrix of diffraction by the HP angle ψ, in normalized coordinates ηL

$$-\sin\gamma\cos\beta\left(\sin\varphi_0-\sin\varphi\right)+$$
$$+\left(\cos\gamma\sin\psi-\sin\gamma\sin\beta\cos\psi\right)\left(\cos\varphi+\cos\varphi_0\right)=0, \quad (6.1)$$

or:

$$tg\gamma=\frac{\sin\psi\left(\cos\varphi+\cos\varphi_0\right)}{\cos\beta\left(\sin\varphi_0-\sin\varphi\right)+\sin\beta\cos\psi\left(\cos\varphi+\cos\varphi_0\right)}. \quad (6.2)$$

Expression (6.2) allows us to define the slope angle γ of the stroke of EDG, the maximum of the diffraction on which is observed at a given value of the HP angle ψ under the other constant CLODL. Together with the expression

$$\chi=\gamma-\alpha, \quad (6.3)$$

where α is the angle of turning of the stereogram around its own normal (to the front-face area) in the right-handed direction, relation (6.2) fixes, under the other constant CLODL, the dependence $\chi(\psi)$ between the division of viewing angle discrete values ψ_n, $n=1,2,...,N$, and the corresponding stroke slope angles χ_n, $n=1,2,...,N$, of the EDGs set, which form stereogram's elemental unit that represents one pixel of each angle shot. Thus, in the general case, the dependence $\chi(\psi)$ is described by the expression

$$\chi=-\alpha+$$
$$+\operatorname{arctg}\left\{\frac{\sin\psi\left(\cos\varphi+\cos\varphi_0\right)}{\cos\beta\left(\sin\varphi_0-\sin\varphi\right)+\sin\beta\cos\psi\left(\cos\varphi+\cos\varphi_0\right)}\right\}, \quad (6.4)$$

which will be used in the stereogram's calculation.

As the stereogram channel, we call the discrete value of viewing at a HP angle. Let us introduce the parameter $s_{n,n\pm1}$ to describe the splitting quality of adjacent [n-th and $(n\pm1)$-th] channels, that is the degree of admixing of the result of diffraction on EDG, which represents the adjacent $(n\pm1)$-th channel, to the result of diffraction on EDG, which represents the given n-th channel under the observation of the diffracting light at the HP angle value ψ_n that corresponds to the diffraction maximum for the given n-th channel:

$$s_{n,n\pm1}=\frac{\left|\eta(\chi_{n\pm1},\psi_n)L\right|}{\pi}=\frac{\left|\eta(\gamma_{n\pm1},\psi_n)L\right|}{\pi}. \quad (7.1)$$

Taking (3.2) and (6.2) into account, we rewrite (7.1) as:

$$s_{n,n\pm1}=-\frac{kL}{\pi}\sin\gamma_{n\pm1}\cos\beta\left(\sin\varphi_0-\sin\varphi\right)+$$
$$+\frac{kL}{\pi}\left(\cos\gamma_{n\pm1}\sin\psi_n-\sin\gamma_{n\pm1}\sin\beta\cos\psi_n\right)\times \quad (7.2)$$
$$\times\left(\cos\varphi+\cos\varphi_0\right).$$

If we have the discrete values ψ_n, $n=1,2,...,N$, of viewing at a HP angle and the corresponding EDGs' stroke slope angles χ_n, $n=1,2,...,N$, or γ_n, $n=1,2,...,N$, [in compliance with (6.3)], then we can calculate the splitting quality of adjacent channels values $s_{n,n\pm1}$, $n=1,2,...,N$.

If the $s_{n,n\pm1}$ parameter takes the integer values, then it coincides by its physical meaning with the number of the minimum (by the HP angle ψ) of the diffraction on the grating of the adjacent $(n\pm1)$-th channel (this minimum is observed at the HP angle ψ that corresponds to the maximum of the diffraction on the grating of the given n-th channel). If values of the $s_{n,n\pm1}$ parameter are semiinteger, i.e. $s_{n,n\pm1}=0.5+m$, $m=1,2,...$, then the $s_{n,n\pm1}-0.5$ parameter by its physical meaning is the number of the maximum (by the HP angle ψ) of the diffraction on the grating of the adjacent $(n\pm1)$-th channel (this maximum is observed at the value of HP angle ψ that corresponds to the maximum of the diffraction on the grating of the given n-th channel). Generally, the parameter $s_{n,n\pm1}$ indicates the relative disposition of zero diffraction maxima (by the HP angle ψ) of adjacent channels; the more this parameter, the better the splitting of channels is observed, i.e. the less the merging of images of adjacent channels occurs.

After the parameters that characterize the EDG's selectivity on the HP angle ψ are defined, we may pass to the calculation of the diffraction on the whole EDG. For that, we have to compute the integral in expression (5.7). As was noticed above, this integral can be determined only for particular shapes of the stroke profile $F_n(y'',z'')=0$ as well as for particular reflectance distributions $\rho(y'',z'')$. Let us consider the rectangular stroke with the reflecting (with reflectance ρ_0) horizontal segments and with completely absorbent vertical segments (Fig. 5). Vertical segments don't contrib contribute to the integral in expression (5.7), inasmuch as $\rho(y'',z'')=0$ for them. Horizontal segments are given by the relation

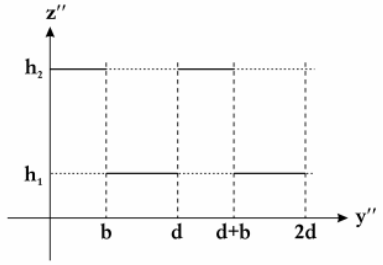

Fig. 5. Reductive presentation of the EDG's stroke

$$F_n(y'', z'') = z'' - h_{1,2} = 0 . \quad (8.1)$$

So, according to (4.7), we have, for horizontal segments,

$$g(y'', z'') = c_2 = -\sin\beta \sin\varphi_0 + \cos\beta \cos\psi \cos\varphi_0 . \quad (8.2)$$

In this case, expression (5.7) which describes the diffraction on one stroke is transformed into the relation

$$u_p = 2LA_1 \frac{\sin\eta L}{\eta L} A_2 c_2 \exp\{i\nu dn\}, \quad (8.3)$$

where

$$A_2 = \frac{\rho_0}{i\nu}\{\exp(i\mu h_2)(\exp(i\nu b) - 1) + \\ + \exp(i\mu h_1)(\exp(i\nu d) - \exp(i\nu b))\} \quad (8.4)$$

is a constant that depends on the stroke parameters. Adding the contributions of n strokes of EDG with regard for:

$$\sum_{n=0}^{N-1} \exp\{i\nu dn\} = \frac{\exp\{i\nu dN\} - 1}{\exp\{i\nu d\} - 1} = \\ = \exp\left\{i\frac{\nu d(N-1)}{2}\right\} \frac{\sin(\nu dN/2)}{\sin\nu d/2}, \quad (8.5)$$

we get the electromagnetic field amplitude of a wave diffracting on EDG at the point P:

$$u_p = 2LA_1A_2A_3 \frac{\sin\eta L}{\eta L} c_2 \frac{\sin(\nu dN/2)}{\sin\nu d/2}, \quad (8.6)$$

where the following designation is introduced:

$$A_3 = \exp\left\{i\frac{\nu d(N-1)}{2}\right\}. \quad (8.7)$$

The term $\frac{\sin(\nu dN/2)}{\sin\nu d/2}$ from expression (8.6) is responsible for the selection of the diffracted light by the wavelength and tops under the following condition:

$$\frac{\nu d}{2} = \pi m, \quad m \in Z . \quad (9.1)$$

Putting ν from (3.2), we can get the following condition for the m-th diffraction maximum in the direction transverse to the stroke line:

Together with condition (6.2) [or (6.4)] of the diffraction maximum in the direction longitudinal for a stroke line, expression (9.2) allows us to determine, for the assigned CLODL $\{\varphi_0, \varphi, \alpha, \beta, \psi_n\}$ and for the color of the n-th angle shot pixel or the wavelength λ of the light diffracting on the EDG which represents this pixel, all the parameters of EDG that must represent the pixel of the n-th angle shot, which is observed at the certain discrete value of the HP viewing angle ψ_n: the stroke slope angle χ_n (the same for all the pixels of the angle shot) and the period d_{nc} that depends on the perspective (ψ_n) and the pixel color (λ) (index c corresponds to color). On the contrary, expression (9.2) allows us to define the wavelength λ of the light diffracting under any CLODL $\{\varphi_0, \varphi, \alpha, \beta, \psi\}$ on the certain EDG with the parameters $\{\chi, d\}$. Expression (8.6) under condition (9.1) becomes

$$u_p = A_E\left[-\sin\beta \sin\varphi_0 + \cos\beta \cos\psi \cos\varphi_0\right]\frac{\sin\eta L}{\eta L}, \quad (10.1)$$

where

$$A_E = \pm 2LNA_1A_2A_3 . \quad (10.2)$$

Intensity I of the light diffracting under the assigned CLODL $\{\varphi_0, \varphi, \alpha, \beta, \psi\}$ on the given EDG $\{\chi, d\}$ at point P can be defined after expression (10.1) is squared:

$$I = A_E{}^2\left[-\sin\beta \sin\varphi_0 + \cos\beta \cos\psi \cos\varphi_0\right]^2\left(\frac{\sin\eta L}{\eta L}\right)^2 . \quad (10.3)$$

We now can sum up the well-handled theoretical discussion of the diffraction on EDG. First, expressions (6.4) and (9.2), which allow one to define the stroke slope angle χ_n and the period d_{nc} for the given discrete value of HP angle ψ_n and fixed CLODL $\{\varphi_0, \varphi, \alpha, \beta\}$, were got. Second, the wavelength λ and the intensity I of the light diffracting on a given EDG with the parameters $\{\chi, d\}$ can be defined for any CLODL $\{\varphi_0, \varphi, \alpha, \beta, \psi\}$ from expressions (9.2) and (10.3). This opportunity allows us to develop the software option of the macrovisualization that models the stereogram behavior or, in other words, represents the result of the diffraction on a stereogram under arbitrary conditions of lighting (by white light) and the observation of the diffracting light in the form of a picture on the display.

$$d = \frac{\lambda}{-\cos\gamma \cos\beta (\sin\varphi_0 - \sin\varphi) - (\sin\gamma \sin\psi + \cos\gamma \sin\beta \cos\psi)(\cos\varphi + \cos\varphi_0)} m, \quad m \in Z \quad (9.2)$$

2.2. Structure of the anigram or the stereogram.

For the multiplex (such as animated or stereographic) images making, the common polygram [1] technology is used. The area of polygram's Elemental Unit (EU) can be divided by the topologies of five different types: ordinary straight diffractive gratings and achromatic straight diffractive gratings, which represent halftone images, curvilinear diffractive gratings representing discs, lenses, and other peculiar images, non-diffractive microstructures and eventually the CGRHs' topology. Every separate topology takes up the adjusted region of an intended EU. EU's separate topology parameters are defined by the color of the image corresponding to an EU pixel, and the presence of a separate topology in a given EU is defined by a mask. Thus, the polygram's structure is determined by the amount and the type of involved images with the related encoding images and image's masks, as well as by EU's masks. EU's mask for all images, except CGRHs, can be of any shape [1]. So, since the anigrams and stereograms are the sets of angle shots – halftone images, the technology of the composite "figure" EU (that is composed from the parts of any shape) for their synthesis and the halftone encoding by the period, filling, or both parameters at once was elaborated, and its software implementation was constructed. Figure 6,a displays the topology of the separate EU of a stereogram (anigram). Evidently, it consists of subregions of an arbitrary adjusted shape. Each subregion of the certain EU represents the certain pixel of each angle shot, i.e. the number of subregions is equal to the amount of stereogram (anigram) channels N; $N = 16$ for the given example. The piece of continuous anigram's topology is depicted in Fig. 6,b. Each subregion of the certain EU is numbered according to the number of the angle shot representing it. The shapes of the corresponding subregions are the same for any EU of the given stereogram (anigram) (or for any image pixel) and don't depend on encoding parameters. The EU depicted in Fig. 6 is reiterated over $ps = 50.0$ mkm in the horizontal and vertical directions. This corresponds to the same pixel size, $ps = 50.0$ mkm, i.e. the resolution of 508 *dpi* of the separate angle shot of a stereogram (or anigram). The angle shots of stereograms are made over the angle distance $\Delta\psi$; in other words, the angle distance between the adjacent discrete values $\psi_n, n = 1, 2, ..., N$ of viewing on a HP angle is equal to $\Delta\psi$. The determination of the optimal ratios of the basic stereogram's parameters as the resolution (or pixel size ps), the number of channels N, and the angle distance $\Delta\psi$ is carried out in Section 3. It is necessary to remark that the halftone encoding consists in the establishment of the accordance between the brightness gr $(gr = 0,1,...,255)$ of a given color channel of the given image and the parameters such as the period, the filling of the intended subregion, achromaticity, and so on of the Diffraction Grating (DG) that occupies the corresponding EU's subregion.

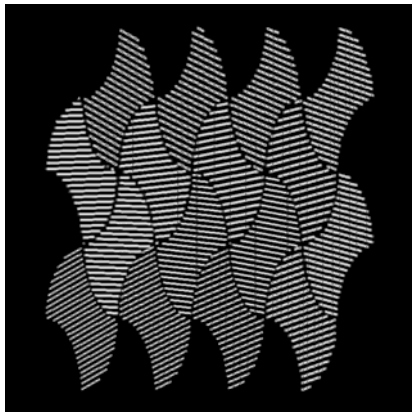

a. single EU

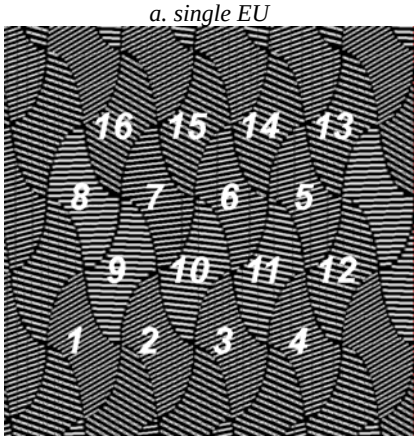

b. EU surrounded by others EUs; EU' numbered subregions

Fig. 6. Structure of anigram's topology

3. Practical results

3.1. Searching for the appropriate synthesis parameters.

Such parameters as the EU's size, or the pixel size ps, and the number of channels N define the area of the EU's separate subregion S under the division of EU into subregions equal by area:

$$S = \frac{ps^2}{N}. \qquad (11.1)$$

The less the subregion area S, the weaker the selectivity on the HP angle of the Diffraction Grating (DG) that fills this subregion (or its part). Let us approximately consider that the DG, which fills a subregion, is equivalent to the square EDG of the same area. The dimension L of such corresponding EDG can be found as:

$$L = \frac{1}{2}\sqrt{S}. \qquad (11.2)$$

By taking (11.1), (11.2), and (6.2) into account, expression (7.2) under the condition $\beta = 0$ can be rewritten as:

$$s_{n,n\pm1} = -\frac{2k \cdot ps}{\pi\sqrt{N}}(\cos\varphi + \cos\varphi_0)\cos\left(\psi_n + \frac{\Delta\psi}{2}\right)\sin\frac{\Delta\psi}{2}, \qquad (11.3)$$

where

$$\Delta\psi = \psi_{n\pm1} - \psi_n . \qquad (11.4)$$

So, according to (11.3), the separation quality $s_{n,n\pm1}$ of the adjacent n-th and $(n\pm1)$-th channels is proportional to ps, inversely proportional to $\lambda\cdot\sqrt{N}$, and approximately proportional to $\Delta\psi$. The parameter $s_{n,n\pm1}$ is the appointing at the synthesis of stereograms (or anigrams). It must be sufficiently large for images in separate channels (angle shots) to be perceived separately, without merging, and, at the same time, sufficiently small for the angle shot to pass and be changed without jumping by another angle shot, i.e. not to disappear before the adjacent angle shot appears. The optimal values of the parameter $s_{n,n\pm1}$ have not defined yet, but the summarizing of the executed investigations allows us to suppose that it must be within the range $0.5 < s_{n,n\pm1} < 1.5$. It is hard to point out the optimal value more accurately, because it can depend on the geometry of stereogram's 3D scene or on parameters of a sequence of anigram's images, the encoding parameters, and so on. The detailed considerations for the accurate determination of optimal values of the parameter $s_{n,n\pm1}$ is planned in the nearest future.

Let us illustrate the behavior of the parameter $s_{n,n\pm1}$ by the following stereogram test recording. It consisted of nine similar cells. The parameters ps and N were $ps = 50.0$ mkm and $N = 16$ for any cell. The 3D scene of one cell was composed from two planes parallel to the hologram plane (Fig. 7). In the upper plane, the set of blue ($\lambda = 436$ nm) rectangles with the side from one to ten pixels was placed, and the set of the yellow ($\lambda = 589$ nm) texts with the line width from one to five pixels was arranged in the lower plane. For each of three values of $\Delta\psi$, $1^\circ, 2^\circ, 3^\circ$, we recorded three cells with different values of the location depth of the defined planes: respectively, $1, 2, 4$ *mm* for the upper plane and $2, 4, 8$ *mm* for the lower one. The values of the parameter $s_{n,n\pm1}$ are presented in Fig. 8.

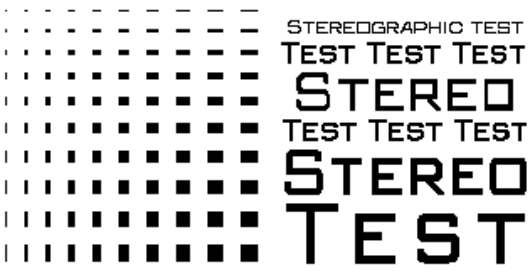

Fig. 7. The upper and lower planes in the cell of the test recording

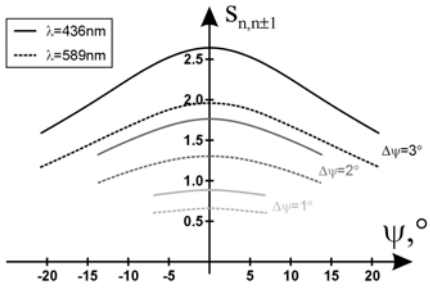

Fig. 8. Values of the parameter $s_{n,n\pm1}$ for the different $\Delta\psi$.

The analysis of test results shows that only the cells in the left column ($\Delta\psi = 1^\circ$, $s_{n,n\pm1} \in (0.8, 0.9)$) work clearly for the rectangles. For other columns, the unpleasant jumping of the brightness with a horizontal viewing angle change is observed. The stereograms of the texts work clearly for the entire left column ($\Delta\psi = 1^\circ$, $s_{n,n\pm1} \in (0.6, 0.65)$) and for depth values up to $4\,mm$ including the middle column ($\Delta\psi = 2^\circ$, $s_{n,n\pm1} \in (1.0, 1.3)$). For the larger depths with a change of the viewing angle, the image sequence itself makes large jumps between the adjacent angle shots, and the illusion of the third dimension disappears. In such a case, it isn't the effect of the parameter $s_{n,n\pm1}$. The range of admissible values of the depth depends on $\Delta\psi$ and on image lines width. The appearance of the image sequence allows us to estimate the depths of the locations of objects admissible or no before the synthesis. The main result of this test recording is that the range of admissible values of the parameter $s_{n,n\pm1}$ was ascertained. The best results in this test were achieved for the range of $s_{n,n\pm1} \in (0.6, 1.3)$.

A good secondary result was obtained: the possibility of achieving the resolution $508\,dpi$ for the stereographic images was confirmed. Indeed, the texts with the line width of one pixel (50 mkm) is discerned completely well.

As concerns the investigation for finding the optimal parameters of the halftone images' encoding, it shows that the encoding of a halftone by the period is better than the encoding by other separate DG's parameter. The best results were observed if the period alters from the black ($gr = 0$, respectively $d = d_{bp}$) to the white point ($gr = 255$, $d = d_{wp}$) with the ratio d_{wp} / d_{bp} which lies in the range $1.4...2.0$. The complex mixed encoding also deserves attention.

We also note that, for hatching images, it's expedient to mark out the background colour and to leave the areas filled in a background color to be empty. This means that some subregions of EU would be empty, and the area of the OSD wouldn't be completely filled.

So, an algorithm of the flexible linking of the stereogram's (or anigram's) channel to the EU's subregion was developed. This algorithm implies the replacement, in a given EU (that corresponds to the image pixel), of the channels with this pixel of a background color by the channels with this pixel of a foreground color. The results obtained for the tough and the flexible linkings of the channel to the subregion of the EU were compared, and it was observed that the flexible filling can give a little gain in the diffraction efficiency.

3.2. Examples of animated and stereographic images.

The opportunities of the presented technology is illustrated by spectacular demonstrational OSDs made by Polygram™ technology: "Galaxy" and "Nature of Optronics" which comprise, as a part, the animated sequences of fractal images and the random abstract background pattern with two blossoming out roses, respectively. They are shown in Figs. 9 and 10.

a) general view

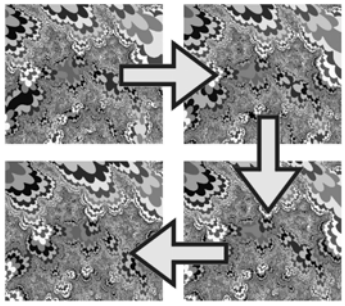

b) some images from sequence

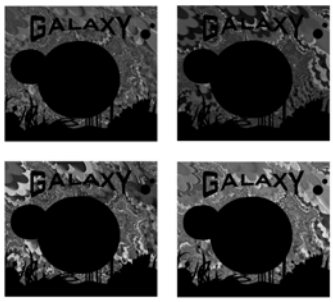

c) macrovisualization results

Fig. 9. Polygram™ "GALAXY" with animated fractal image

a) general view

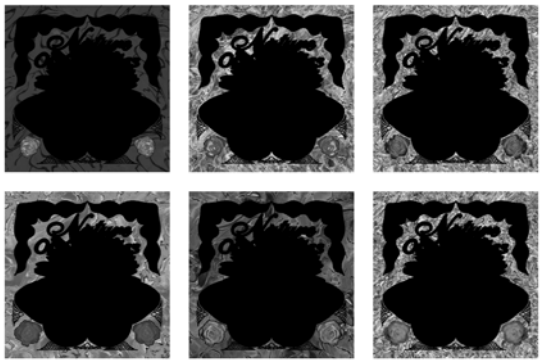

b) macrovisualization results

Fig. 10. Polygram™ "Nature of Optronics" with animated image of blossoming out roses

4. Conclusions

In the present paper, the theory and the practice of stereographic and animated rainbow diffractive images making have been expounded. So, the basic parameters essential for the multiplex images making are determined, and the examples of such images are given. But some items that can be improved have still remained.

So, it is necessary to consider the diffraction on the reflective phase EDG placed not only in vacuum but also under a thin film or layer. The rules for finding the optimal values of the adjacent channels separation quality (parameter $s_{n,n\pm1}$) can be defined more exactly.

Moreover, the influence of the stereogram's scene space geometry or the parameters of anigram's images sequence on the optimal angle distance between them ($\Delta\psi$) needs to be explored, and the range of the admissible values of these parameters must be determined. The encoding methods aren't explored exhaustively.

But, nevertheless, the developed technology has already suited perfectly for making spectacular and sufficiently reliable multiplex images. The substantial development of the presented technology promises to bring up the exact precepts how to achieve the maximum visual effect and to make these images especially vivid and unusually impressive.

References

1. V. Girnyk, S. Kostyukevych, A. Kononov, I. Borisov "Application of computer-generated rainbow holograms of 3D images in optical security devices," *SPIE Proceedings* **5005**, pp.338-344, 2003.
2. V. Girnyk, S. Kostyukevych, A. Kononov, I. Borisov "Multilevel computer-generated holograms for reconstructing 3D images in combined optical-digital security devices," *SPIE Proceedings* **4677**, pp.255-266, 2002.
3. T. Hamano, H. Yoshikawa, "Image-type CGH by means of e-beam printing," *SPIE Proceedings* **3293**, pp.2-14, 1998.
4. T. Hamano, H. Yoshikawa, "Computer-generated holograms with pulse-width modulation for multi-level 3D images," *SPIE Proceedings* **3637**, pp. 244-251, 1999.
5. T. Hamano, M. Kitamura, "Computer-generated holograms for reconstructing multi 3D images by space-division recording method," *SPIE Proceedings* **3956**, pp. 23-32, 2000.
6. M. Lucente, "Interactive computation of holograms using a look-up table," *SPIE Proceedings* **1667**, 1992.
7. D. Leseberg, "Computer-generated three-dimensional image holograms," *Appl. Opt*. **31**(2), pp. 223-229, 1992.
8. A. W. Lohmann, S. Sinzinger, "Graphic codes for computer holography", *Appl. Opt.* **34**(17), pp. 3172-3178, 1995.
9. H. Yoshikawa, H. Taniguchi, "Computer-generated rainbow hologram," *Opt. Rev*. **6**(2), pp. 118-123, 1999
10. Ilya S. Borisov, Valeriy I. Grygoruk, Sergey A. Kostyukevych, Physical aspects of digital synthesis and reconstruction of the multiview diffractive images, Proc. SPIE Vol. 6136, 61360A, Practical Holography XX: Materials and Applications; Hans I. Bjelkhagen, Roger A. Lessard; Eds., Feb 2006.
11. Vladimir I. Girnyk, Sergey A. Kostyukevych, Eugene V. Braginets, Alexander A. Soroka, 3D CGH registration on organic and non-organic resists: comparative analysis, Proc. SPIE Vol. 6136, 61360P, Practical Holography XX: Materials and Applications; Hans I. Bjelkhagen, Roger A. Lessard; Eds., Feb 2006.